AIAA 2001-2921

On the Use of Surface Porosity to Reduce Unsteady Lift

Ana F. Tinetti, Jeffrey J. Kelly
Virginia Polytechnic Institute and State University / VCES
Hampton, VA

Steven X. S. Bauer, Russell H. Thomas
NASA Langley Research Center
Hampton, VA

31st AIAA Fluid Dynamics Conference and Exhibit
11-14 June 2001 / Anaheim, CA

AIAA 2001-2921

ON THE USE OF SURFACE POROSITY TO REDUCE UNSTEADY LIFT

Ana F. Tinetti*, Jeffrey J. Kelly†
Virginia Polytechnic Institute and State University, VCES
Hampton, VA. 23666

Steven X. S. Bauer‡, Russell H. Thomas§
NASA Langley Research Center
Hampton, VA. 23681

Abstract

An innovative application of existing technology is proposed for attenuating the effects of transient phenomena, such as rotor-stator and rotor-strut interactions, linked to noise and fatigue failure in turbomachinery environments. A computational study was designed to assess the potential of passive porosity technology as a mechanism for alleviating interaction effects by reducing the unsteady lift developed on a stator airfoil subject to wake impingement. The study involved a typical high bypass fan stator airfoil (solid baseline and several porous configurations), immersed in a free field and exposed to the effects of a transversely moving wake. It was found that, for the airfoil under consideration, the magnitude of the unsteady lift could be reduced more than 18% without incurring significant performance losses.

Nomenclature

A Cross sectional area
LE Leading edge
M Local Mach number
Re Reynolds number
Sn Strouhal number, $Sn = (\omega d)/(2\pi U)$
T Local temperature
U Freestream velocity
V Wake translational speed
c Airfoil chord
c_d Airfoil drag coefficient
c_l Airfoil lift coefficient
c_p Airfoil pressure coefficient
d Diameter of wake generator
p Local flow static pressure
s Solidity, seconds
t time
u Local flow velocity normal to porous surface
x Axial or chordwise distance
ϕ Contraction coefficient
γ Ratio of specific heats, $\gamma = 1.4$ for air
ρ Local flow density

Subscripts

1 Upstream of porous surface
2 Minimum area of flow through porous surface
3 Fully mixed flow region, downstream of surface
c Closed (area)
max Maximum value
min Minimum value
o Open (area)
t Stagnation condition
∞ Freestream quantity
0 Start of wake traverse, t = 0.0 seconds
s Solid stator
w Wake effects

Introduction

Porous media, such as screens and perforated plates, have been widely used in fluid dynamics studies since the 1940s[1]. These applications mostly occurred in the areas of production/reduction of turbulence and the creation/elimination of large scale velocity or pressure non-uniformities. Important examples are the use of screens to minimize flow turbulence in wind tunnels[2], applications in boundary layer control[3, 4], and reduction of aerodynamic forces. In the latter application, the porous medium is in the form of a perforated outer surface, exposed to the flow at any given incidence. The system also includes a solid inner surface such that the volume between the two forms a plenum that is filled with the same fluid flowing over the outer surface[5]. This arrangement, known as passive porosity, redistributes pressure on the outer surface by establishing communication between regions of high and low pressure through the plenum. The pressure redistribution, which is associated with a minute transfer of mass into and out of the plenum, changes the effective aerodynamic shape of the outer surface. Passive porosity has been used to reduce wave drag and delay buffet onset in transonic airfoils by reducing shock-boundary layer interaction[6,7], and to

* Research Assistant, Mechanical Engineering Department, Senior Member AIAA.
† Research Associate Professor, Mechanical Engineering Department, Senior Member AIAA.
‡ Senior Research Engineer, Configuration Aerodynamics Branch, Associate Fellow AIAA.
§ Aerospace Engineer, Aeroacoustics Branch, Senior Member AIAA.

reduce large side forces in bodies of revolution at high angles of attack caused by asymmetric pressure loading due to flow separation[8]. Passive porosity has also been used to reduce blade-vortex interaction (BVI) in rotorcraft[9]. In turbomachinery, it can be applied to the reduction of phenomena associated with unsteady flow such as rotor-stator and rotor-strut interactions, which are directly related to fan noise and can cause high cycle fatigue failure.

The nature of the unsteady flow in turbomachines is usually determined by circulation effects, blade thickness effects, and wake effects[10,11]. The circulation effect is caused by the presence of circulation around the moving wake-generating blades, and it can be neglected when compared to wake effects if the distance between the wake generator and the stator is more than 10% - 20% of the stator chord. Blade thickness effects are caused by the interaction between potential (inviscid) flow fields around rotor blades of finite thickness. This effect is important when the distance between the rotor and stator is less than approximately one airfoil chord. The wake (viscous) effect is caused by wake-stator interactions that form as the wakes shed from the upstream rotor impinge on, and then convect past, the downstream stator. Since the wake rate of decay is much slower than that of the potential flow interactions, wake effects can still be significant several chord lengths downstream. Note that this effect would be zero in an inviscid fluid, since wakes are direct consequences of the boundary layer development on the generating body. These three effects contribute to momentary changes in local flow incidence and magnitude that give rise to variations in surface pressure (i.e., lift). However, the wake effect is by far the most important of the three.

The aerodynamic parameters associated with rotor-stator and rotor-strut interactions can be grouped into those that (1) would reduce the wakes shed by the rotors, and (2) would reduce the response of the stators and struts to impinging wakes. Any approach designed to alter these groups must do so within the confines of acceptable performance losses. For turbomachinery applications, the overriding concern is the minimization of flow separation on rotor and stator surfaces. Passive porosity technology can be used to modify both groups, the first by reducing wake velocity defect and width through reductions in rotor drag, and the second by reducing the stator/strut response through reductions in fluctuating lift. The latter application is the subject of the present study.

Porous Surface Model

The porosity model used in this investigation was developed in reference 12 from normal screen loss analytical and experimental results presented in reference 13. If the perforated plate is considered to produce a series of jets that coalesce gradually in the downstream direction, three uniform states can be determined (Figure 1): the free stream well ahead of the screen (1), the location of minimum area at which the jets formed by the screen holes are fully contracted but essentially undiffused (2), and the free stream well beyond the screen where the flow is fully mixed (3). The upstream and downstream areas are equal. The area at 2 is reduced by the solidity s and a contraction coefficient ϕ. Thus,

$$A_1 = A_3 \qquad (1)$$

$$A_2 = A_1\phi(1 - s) \qquad (2)$$

where

$$s = \frac{A_c}{A_c + A_o} \qquad (3)$$

The contraction coefficient ϕ is given by[14]

$$\phi = \phi_o + 0.185s^{0.25}\left(\frac{p_{t2}}{p_2} - 1\right) \qquad (4)$$

where the empirical incompressible component ϕ_0 is

$$\phi_o = \frac{0.04137}{1.0982 - (1 - s)} + 0.57323 + 0.005786(1 - s) \qquad (5)$$

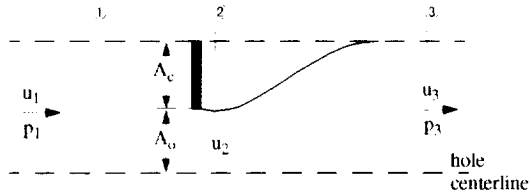

Figure 1.- Model of flow through a single screen hole.

The governing equations are derived from conservation of mass and momentum laws for the steady, one-dimensional, isentropic (adiabatic and reversible) flow of a perfect gas. It is also assumed that there is no total pressure loss during jet formation. This assumption is valid as long as the fluid passing through the hole has an inviscid core. Thus, the flow normal to the porous surface is given by

Conservation of mass:

$$(\rho u)_1 = (\rho u)_2\phi(1 - s) = (\rho u)_3 \qquad (6)$$

Conservation of momentum:

$$p_1(1+\gamma M_1^2) = p_2[1+\gamma M_2^2\phi(1-s)] = p_3(1+\gamma M_3^2) \quad (7)$$

Adiabatic flow:

$$T_{t1} = T_{t2} = T_{t3} \quad (8)$$

Zero total pressure loss:

$$p_{t1} = p_{t2} \quad (9)$$

The model is implemented as a surface boundary condition with the aid of two additional assumptions: first, the process from state 1 to state 3 takes place over an infinitesimal distance; second, the pressure inside the plenum is constant. As a result, only the flow side of the porous surface needs to be gridded, and all the information necessary to describe the process is obtained from the known mass flow in the computational domain and a given plenum pressure.

Assuming that a pressure gradient exists across the porous surface, the local flow will enter the plenum if $p_{domain} > p_{plenum}$, and exit the plenum if the converse is true. The plenum pressure at every global iteration is found by averaging the known surface pressures in the computational domain over the area covered by a given porous patch. As the solution converges, the plenum pressure reaches a steady value for which the net mass flux across the porous surface approaches zero. Detailed descriptions of the model implementation and validation are given in reference 14.

Computational Tools

Flow Solver

CFL3D[15], developed at the NASA Langley Research Center, was used to calculate the results presented in this paper. The code solves the three-dimensional, time-dependent, thin-layer approximation to the Reynolds-Averaged Navier-Stokes (RANS) equations using a finite volume formulation in generalized coordinates. It uses upwind-biased spatial differencing with Roe's flux-difference splitting (FDS) method[16] for the inviscid terms, and central differences for the viscous and heat transfer terms. The code, which is second-order accurate in space, is advanced in time with an implicit three-factor approximate factorization (AF) scheme. Temporal subiterations with multigrid are used to recover time accuracy lost as a result of the AF approach during unsteady calculations. The pseudo-time subiteration (τ-TS) method is used in the present work. In this option, a pseudo-time term is added to the time-accurate Navier-Stokes equations. This extra term is sub-iterated until acceptable convergence is obtained. Good convergence was reached using five subiterations for each physical time step. CFL3D includes several grid connection strategies, a vast array of zero-, one-, and two-equation turbulence models (linear as well as nonlinear), numerous boundary conditions, and translating grid capabilities suitable for turbomachinery applications. The results presented here were obtained using the two-equation k-ω SST model of Menter[17].

Structured Grid

The problem of trying to numerically simulate the aerodynamic environment within a turbofan is inherently difficult. However, it can be greatly simplified by considering a system composed of a single rotor blade (or any other suitable wake generator) transversely moving past a single stator vane. Wake effects would still be the main cause of unsteadiness within such a system. Thickness effects, although still present, would be small in comparison to wake effects if the distance between the rotor and the stator leading edge is approximately 40% of the stator chord[10]. Circulation effects would be insignificant at this distance. Furthermore, three-dimensional effects such as blade tip and cross-flow effects can be avoided if the system is made two-dimensional. Thus, the computational setup chosen for the study consists of a single stator airfoil immersed in a free flow field, subject to the effects of a transversely moving wake. Schematic representations of the grid, airfoil, and wake are given in Figure 2.

The 9-zone, 2-D grid contains approximately 2.39×10^5 points/plane, extending to 15c above and below the airfoil, 0.26c upstream and 2.5c downstream. Far field boundary conditions are applied at the external faces of the grid, interface boundary conditions are applied at all the internal faces, and viscous and porous surface boundary conditions are applied at the airfoil surface. The vertical extension of the grid, in conjunction with a stretched distribution of points toward the far field, are required in order to dissipate reflections from the boundaries. The majority of the grid points are contained in zones 1, 4, and 3, as is necessary to ensure adequate propagation of perturbation waves.

The chosen airfoil was obtained from surface measurements taken at the mid-span of one of the stator vanes composing the Pratt and Whitney Advanced Ducted Propeller high power fan model currently at NASA LaRC[18]. Leading and trailing edges were not defined. Thus, they were created by carefully fitting circular arcs to the given discrete points. Since the section would no longer function as part of a stator vane, its incidence had to be

adjusted in order to preclude flow separation over its surface. Results from an angle of attack sweep indicated that there exists a narrow incidence range within which the flow would remain attached over the entire airfoil surface. The mid-point of that range, 6°, was selected.

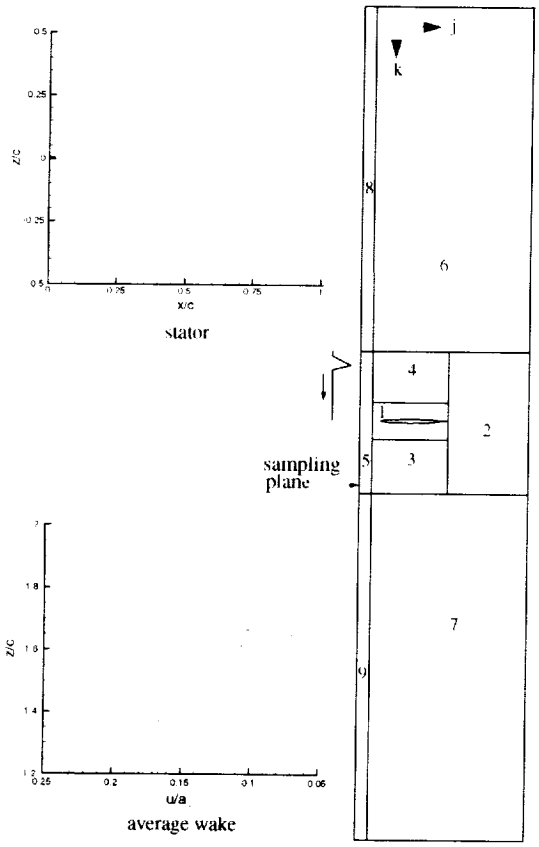

Figure 2.- Computational grid.

Because a strong wake was desired, a cylinder (not shown) with a diameter of approximately 0.05c, and located 0.41c upstream of the stator LE plane, was used initially as a wake generator. Although a satisfactory wake was obtained, its effect on stator lift was heavily influenced by the vorticity resulting from the Karman vortex street characteristic of flow over blunt bodies. The effect of the shed vortices manifested itself as oscillations in c_l with frequencies corresponding to Sn ~ 0.2. In order to eliminate these unwanted oscillations, an average profile was obtained from several temporal samples of the wake generated by the rod as it approached and passed the stator. This average wake, which has a 33% velocity defect at the plane of the stator LE, represented tremendous savings in computing time, since the zones defining the rod would no longer be necessary. The average wake, now a user input, is defined at the sampling plane (face j1 of zone 5, 0.15c downstream of the original rod) using a velocity distribution boundary condition. Through the use of dynamic patched interfacing, this wake is displaced a distance of approximately 4c, from face k1 to face kmax of zone 5, by a downward translation of zones 5, 8 and 9. At the end of the specified traverse, the algorithm translates the moving blocks and their solution back to their original position.

To minimize numerical dissipation as the wake traverses the stator flow field, the axial distance between the plane of the wake and the stator LE is kept as small as possible, and the cell size ratio between the zones defining the wake and the stator does not exceed 3:1 during the entire wake traverse. A translational speed (V) of 78c/s, corresponding to an angular velocity of 500 rpm and a mid-span radius of 1.5c, was chosen for the wake. The entire wake traverse requires 2232 time steps. The given translational speed, traversed distance, and free stream Mach number (0.166) guarantee that, at any given time, the stator is subject to the passage of a single wake only.

Results and Discussion

Effect of Moving Wake on Airfoil Surface Pressure

The effect of the moving wake on the flowfield around the stator leading edge is sequentially depicted in Figures 3a through 3d. Corresponding surface pressure coefficient distributions are presented in Figure 4. In general, the pressure on the convex surface of a stator vane (or rotor blade) is relatively low, and the pressure on the concave side is relatively high. For this reason, the convex and concave surfaces are usually called the suction and pressure sides, respectively, of the stator. The process described here is common in turbomachinery flows[10,11,19,20].

At the start of the traverse, t = 0.0 seconds (Figure 3a), the wake is located approximately 2c above the stator. This relative placement precludes any significant interaction between the two. The associated surface pressure distribution is as would be expected for the airfoil immersed in a free stream at the chosen incidence. Note from Figure 4 that surface pressure is minimum at the 40% chord location, coincident with the point of maximum airfoil thickness. The recompression of the surface pressure downstream of the maximum thickness location indicates that the flow remains attached over the entire airfoil surface. Close examination of the flow past the TE revealed that the "blip" in the c_p distributions results from a combination of airfoil incidence and TE geometry, and is not an indication of flow separation.

The point of maximum pressure is located at the stator L.E. Because of the airfoil positive incidence, a point of local minimum pressure, a direct consequence of local flow expansion, is located on the suction (leeward) side at x/c ~ 0.003.

The flow around the stator remains virtually unaffected by the moving wake until approximately t = 0.0176 s (Figure 3b). After this time, the close proximity of the wake to the stator L.E causes a gradual decrease in the local flow incidence. At time t = 0.0229 s, the wake intersects the stator L.E (Figure 3c) causing a large reduction in Δc_p that extends over 90% of the airfoil. The change in relative wind incidence shifts the stagnation point from the origin (x/c = z/c = 0) to the suction side of the airfoil, and the point of local minimum pressure from the suction side to the pressure (windward) side. In the immediate vicinity of the wake, as it passed over the airfoil, the velocity was seen to decrease and then increase on the suction side, and, conversely, to increase and then decrease on the pressure side. As a consequence, the pressure rises and then falls on the suction side, and falls and then rises on the pressure side. This behavior is clearly seen in the surface c_p distributions of Figure 4. The process is then reverted as the wake moves past the stator airfoil (Figure 3d).

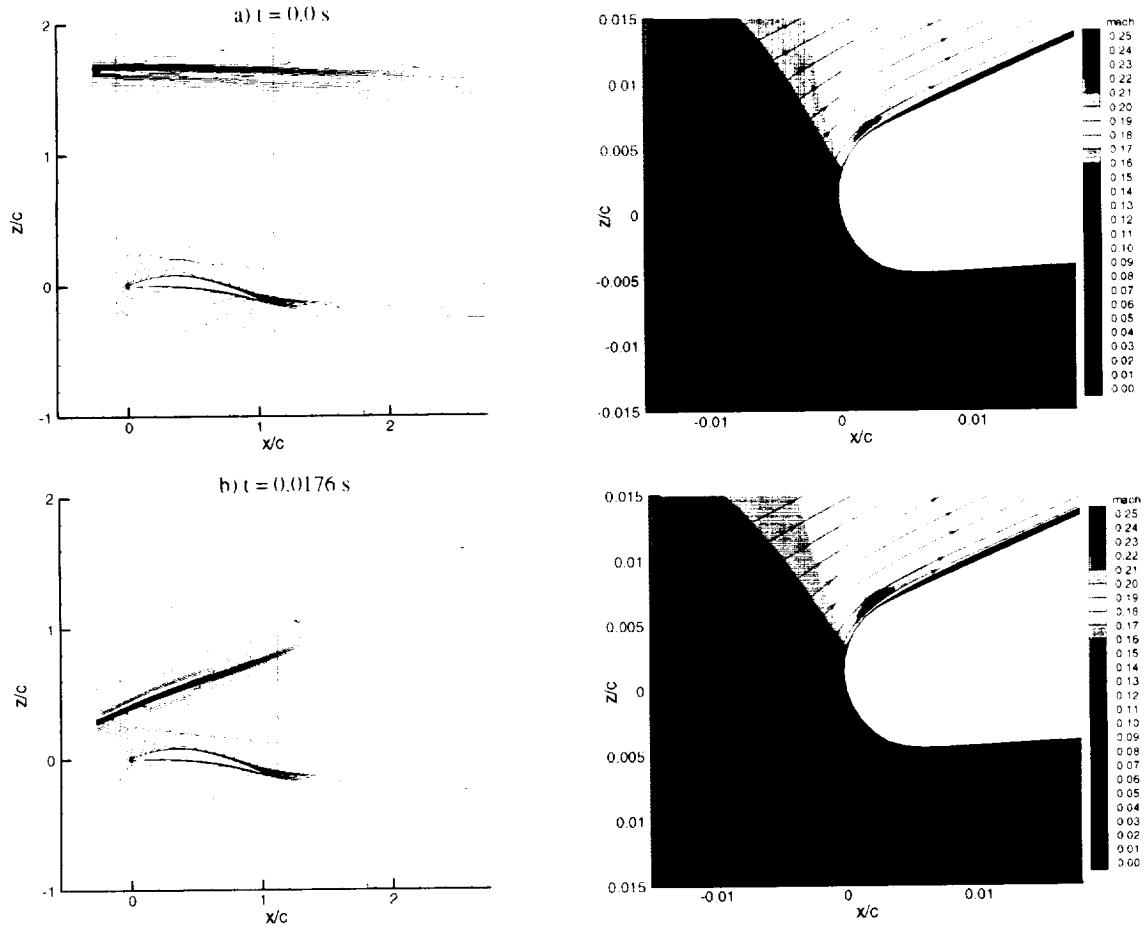

Figure 3.- Mach Number contours for solid stator. $M_\infty = 0.166$, $Re = 1.125 \times 10^6$, $\alpha = 6^\circ$, V = 78c/sec. Medium grid level.

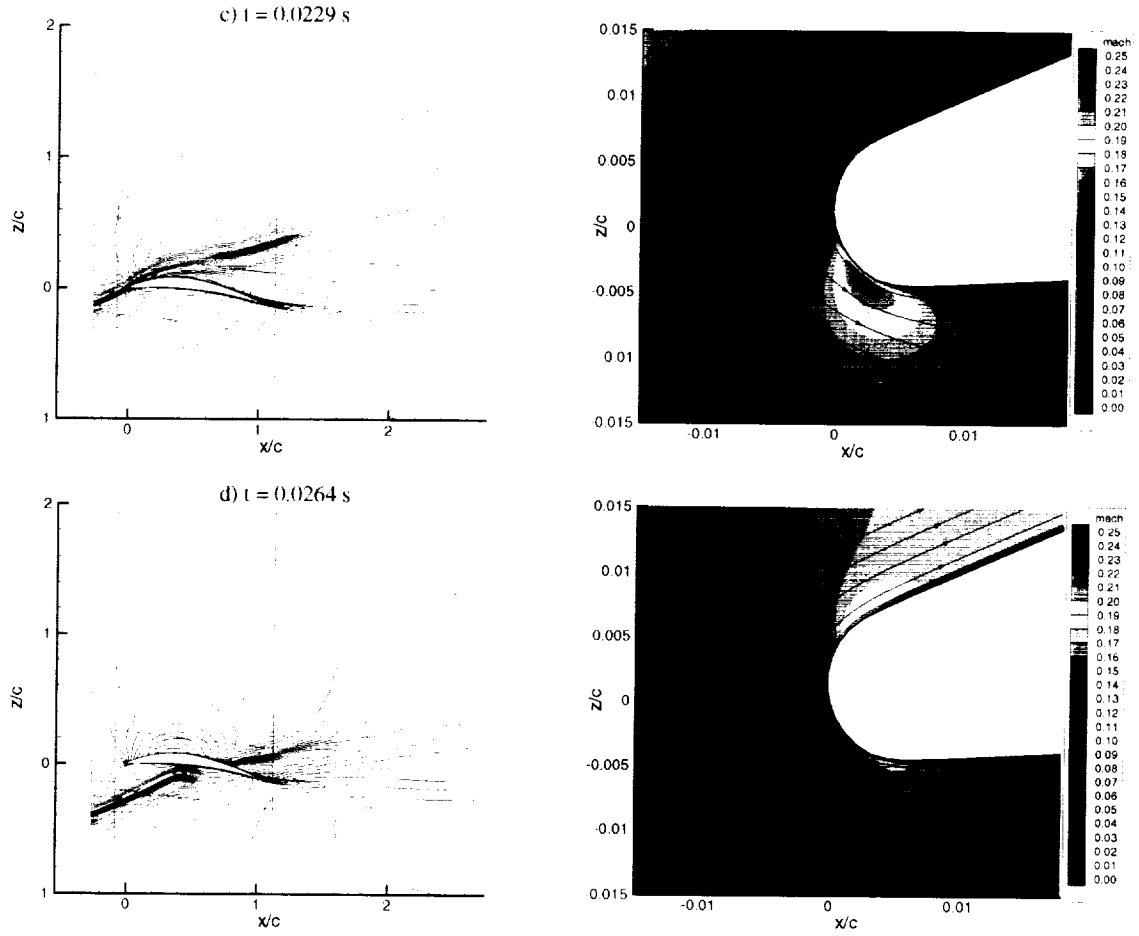

Figure 3.- Concluded.

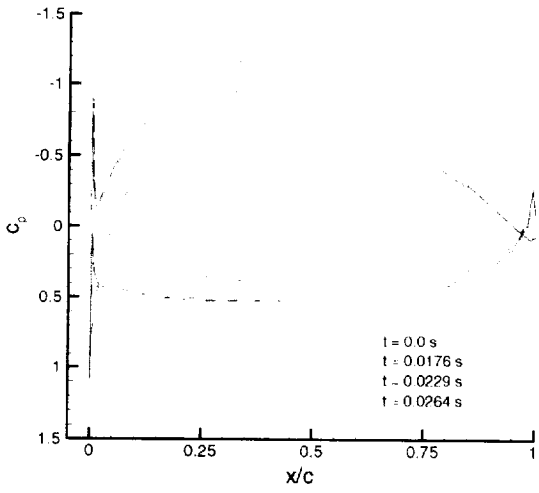

Figure 4.- Surface pressure coefficient distribution for solid stator airfoil, medium grid level. $M_\infty = 0.166$, $Re = 1.125 \times 10^6$.

Effect of Moving Wake on Airfoil Lift

The unsteady nature of the lift generated by a solid stator when subjected to wake convection is depicted in Figure 5. Note from the figure that the lift coefficient decreases as the wake approaches the stator, reaches a minimum at the point of closest approach between the wake and the stator LE (t = 0.0229 s), and then recovers as the wake recedes until levels similar to those existing at the start of the traverse are established. This behavior is directly related to the changes in pressure over the airfoil surface caused by the presence of the wake. As the wake moves past the stator, the local flow undergoes transient fluctuations in velocity and turbulence intensity that affect the boundary layer, and consequently, the surface pressure distribution.

The maximum variation in c_l resulting from wake-stator interaction effects can be defined as

$$(\Delta c_{l_w})_{max} = \frac{(c_{l_s})_0 - (c_l)_{min}}{(c_{l_s})_0} \qquad (10)$$

In the above equation, $(c_{l_s})_0$, the solid stator c_l value at the start of the wake traverse (t = 0.0 s), was obtained from a converged solution with the wake held stationary at a distance of approximately 2 chords above the airfoil. $(c_l)_{min}$ is the minimum c_l value associated with wake convection. Thus, for the solid stator airfoil, $(\Delta c_{l_w})_{max}$ is 29%.

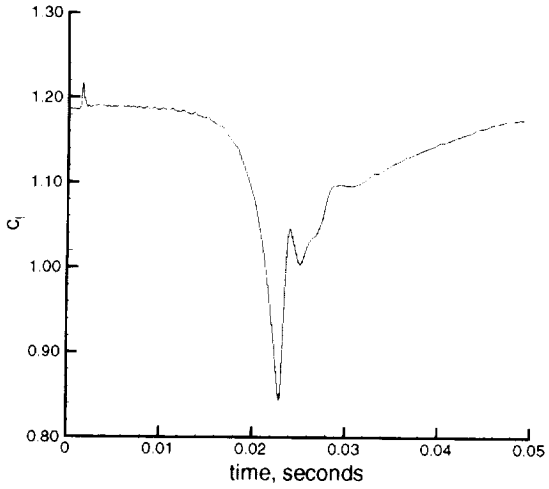

Figure 5.- Effect of wake passage on stator lift coefficient, fine grid level, M = 0.166, Re = 1.125×10^6, V = 78c/s

Effect of Surface Porosity on Airfoil Pressure

The extent and location of the porous regions will depend, of course, on the intended application. For the reduction of unsteady interactions in turbomachinery environments, the overriding performance concern is the minimization of flow separation on the stator surfaces. A parametric study involving 45+ different porous configurations was performed in order to isolate those that would minimize the change in lift caused by wake convection, without compromising airfoil performance. The variable parameters were the extent and location of the porous patches (ranging from full-chord porosity to small isolated regions near the LE and TE), the configuration of the assumed plenum chamber (single or multiple, either connected or disconnected), and the surface porosity (either constant or tapered with distance along the surface). A value of 22% porosity[8] was chosen as a basis.

The study showed that as long as the porous patch on the leeward side does not extend past the 10% chord location, the flow remains attached over the entire airfoil surface. It was also found that, because of airfoil geometry, the porosity on the leeward side had to be tapered from the nominal to less than 10% in the region $0.05 \leq x/c \leq 0.10$ in order to preclude the formation of a small recirculation area immediately downstream of the porous patch. Variations in porosity of ±10% from the basis had a small effect on airfoil lift. The configurations yielding the largest unsteady lift reductions were those that involved communication, through the plenum, between regions of high pressure differential ahead of x/c = 0.15.

Some of the viable configurations obtained during the parametric study are presented next. The series, shown in Figure 6, has a leeward side porosity distribution of 22% in the region $0 \leq x/c < 0.05$, then tapered elliptically from 22% to 10% in the region $0.05 \leq x/c \leq 0.10$. It also includes an isolated 22% porosity patch in the region $0.95 \leq x/c \leq 1.0$ aimed at alleviating TE flow separation. It has been determined that this patch is not necessary, since, in general, the viable configurations do not induce flow separation. However, it was included early in the study and kept for some of the configurations. Its effect is negligible. The porosity distribution on the windward side consists of a 22% porous patch with an extension that varies from 10% of the chord up to 25%, 50% and full-chord, for configurations A, B, C, and D, respectively. The main porous region in each configuration is continuous, i.e., it is defined as a single patch with a single implicit plenum chamber.

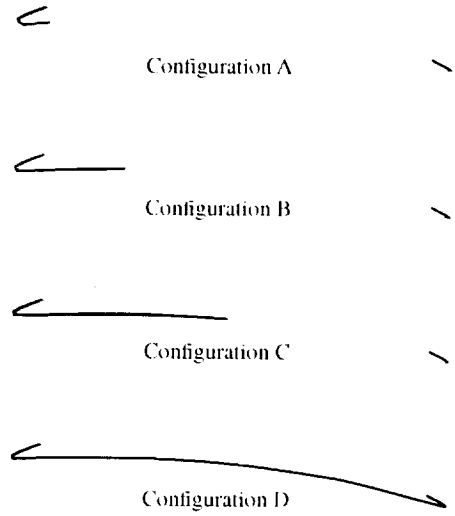

Figure 6.- Sample porous distributions.

The effect of porosity on the flow in the vicinity of the stator LE is depicted in Figure 7, for t = 0.0 s. Wake-stator interaction effects are negligible. The small amount of mass transfer characteristic of passive porosity is represented by velocity vectors whose length, amplified several times for visualization purposes, is proportional to the magnitude of the flow normal to the surface. Corresponding surface pressure coefficient distributions are also presented in the figures. The flow around the solid stator LE (Figure 7a) is provided as a reference.

Porosity alters the effective aerodynamic shape of a body by modifying the pressure distribution over its surface. As expected, these changes affect the flow in the vicinity of the body. The expected effect of porosity on the local flow in the vicinity of the leading edge of an airfoil is the creation of stable regions of inflow ($p_{plenum} < p_{domain}$) in areas of high surface pressure, and outflow ($p_{plenum} > p_{domain}$) in areas of low surface pressure. These high and low pressure areas are usually located on the windward and leeward surfaces of the airfoil, respectively. In regions of inflow, some of the decelerated fluid particles in the boundary layer are removed, resulting in a thinner boundary layer. In regions of outflow, additional energy is supplied to the fluid particles being retarded, resulting in the creation of a sub-layer near the wall that reduces shear forces and displaces the boundary layer away from the surface. However, the numerical results presented here indicate that porosity tends to induce a time-dependent oscillatory pattern of small inflow-outflow regions near the stator leading edge, which is well established before wake effects come into play.

The causes of the oscillatory pattern are not well understood, but are most likely related to airfoil geometry and flow incidence. As mentioned earlier, an analytical definition for the airfoil was not available. Thus, a circular arc was fitted to the given discrete points to form a LE. Although the fitting process was carefully done, minute slope discontinuities could not be avoided. Because the airfoil is subject to off-design conditions, atypically low levels of lift are generated at the LE, as seen in the c_p distribution for the solid airfoil (Figure 7a). It is possible that the combined effect of these two factors triggered the oscillatory inflow-outflow pattern shown here.

The periodic, oscillatory pattern starts at the LE, where air always flows into the plenum, and travels downstream on both leeward and windward sides of the airfoil. On the leeward side, the pattern travels to the aft end of the patch and beyond. This additional distance depends on the extension of the patch on the lower surface, but is between an extra 0.05c for configuration A to about an extra 0.20c for configuration D. The amplitude of the disturbances peaks at the aft end of the patch (x/c = 0.1) for all configurations, and diminishes from there. On the windward side of the airfoil, the disturbances travel to approximately 50% of the patch extension. Their amplitude peaks shortly aft of the LE, and diminishes as the disturbances travel downstream. One period of this oscillatory pattern is presented in Figure 8, for configuration A. The period considered in the figure is early during the wake traverse in order to exclude wake-stator interaction effects.

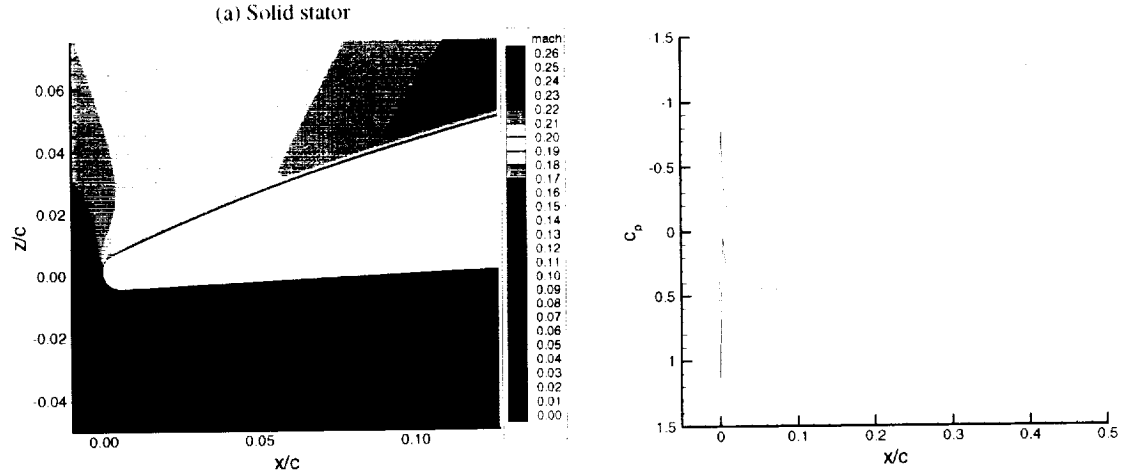

Figure 7.- Effect of surface porosity on Mach number contours and surface pressure distributions for flow around the stator LE at t = 0.0 s. Medium grid, $M_\infty = 0.166$, $\alpha = 6^o$.

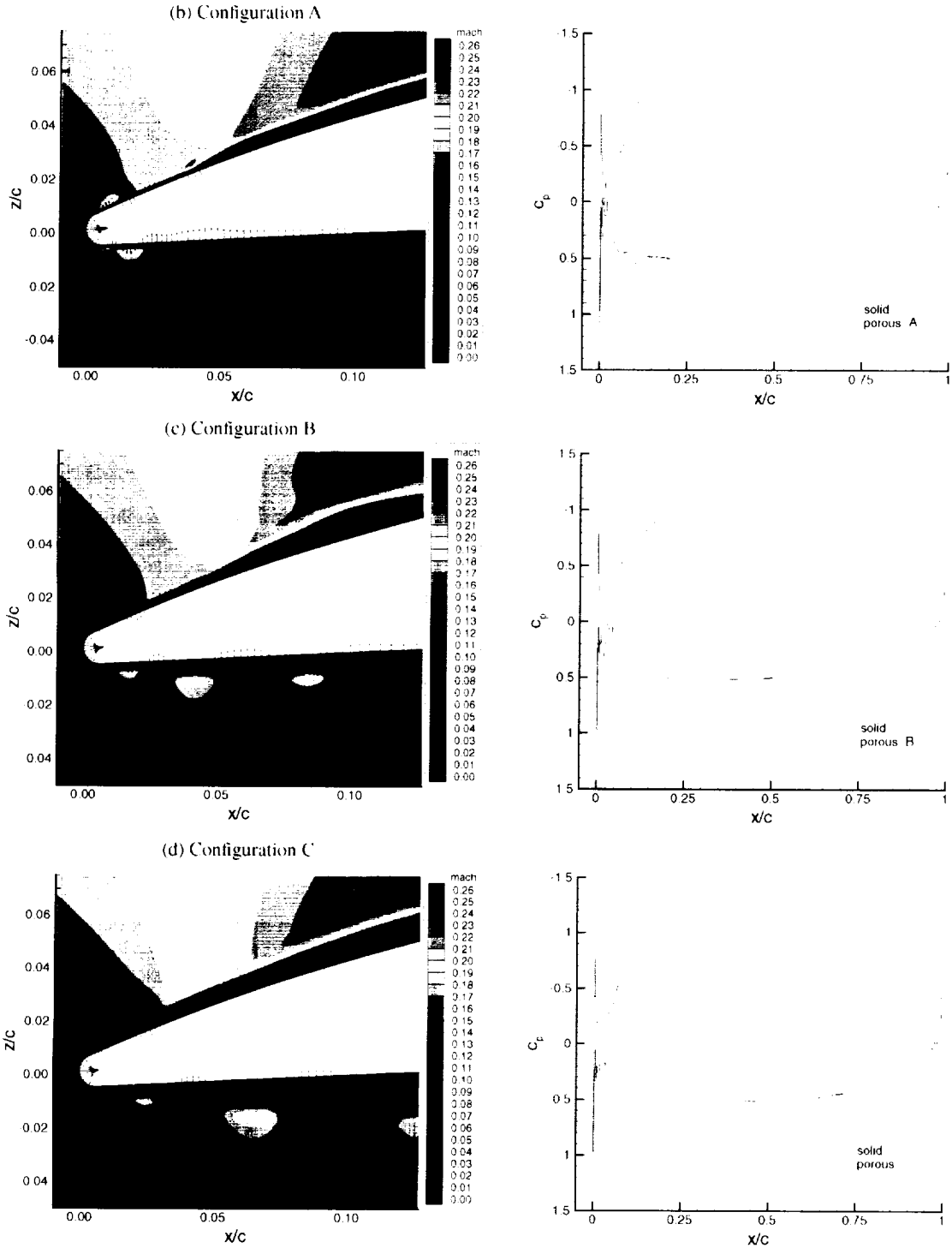

Figure 7.- Continued.

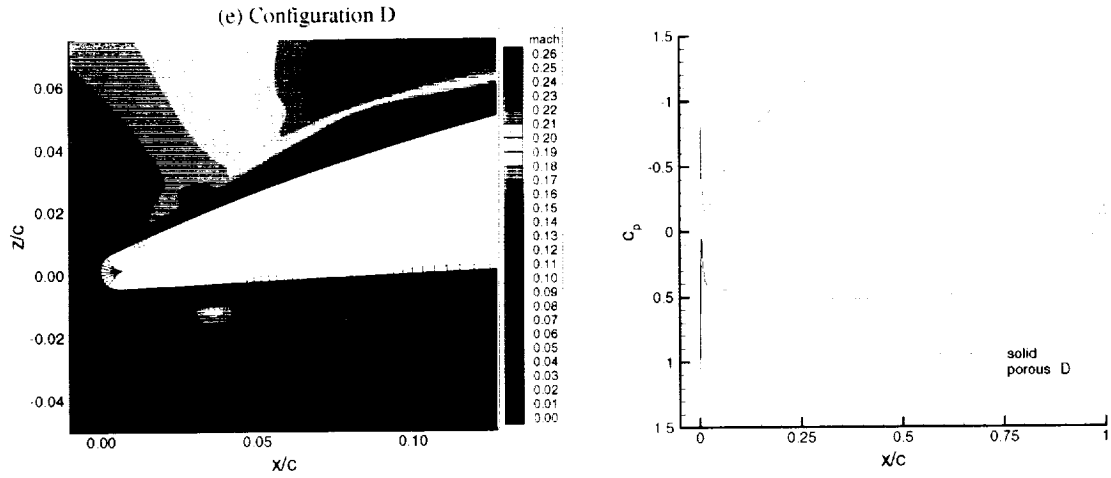

Figure 7.- Concluded.

Regardless of the unsteadiness caused by the periodic inflow-outflow oscillations, it can be seen from the pressure distributions that the flow remains attached over the entire surface for all configurations except D, for which the flow over the leeward side has slightly separated in the TE region.

The periodic, oscillatory behavior described here would probably not arise if the airfoil were placed within a stator cascade, and subject to flow conditions typical of turbomachinery environments. However, it has been observed experimentally during an internal NASA LaRC wind tunnel test of a spherical nose/cylinder forebody model with equivalent porosity levels[21].

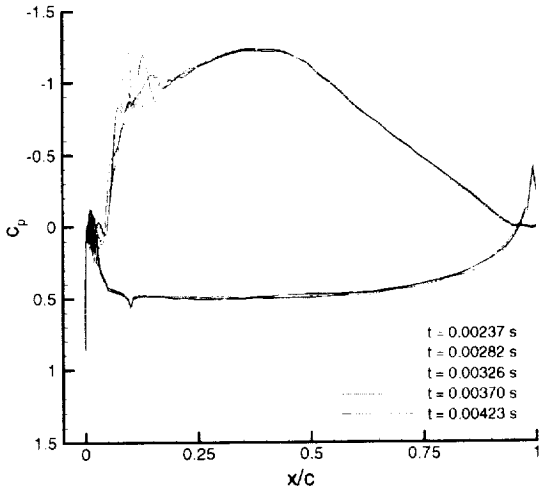

Figure 8.- Effects of porosity-induced flow unsteadiness on surface pressure distribution, configuration A. Medium grid level. $M_\infty = 0.166$, $Re = 1.125 \times 10^6$.

Effect of Moving Wake on Porous Airfoil Behavior

It has been observed from surface pressure animations (not shown) that wake-stator interaction tends to reduce the amplitude of the porosity-induced oscillations on the leeward side of the airfoil. For configuration A, which has the least amount of porosity, the strength of the interaction is sufficient to cancel the oscillations after the wake intersects the stator LE. The cancelling effect of the interaction decreases as the extension of the patch on the windward side increases. For configuration D, wake impingement momentarily halts the oscillatory behavior over the patch surface. However, it starts immediately aft of the patch, and travels downstream on the displaced boundary layer an additional 0.1c. After a while, the behavior observed prior to wake approach reestablishes itself.

Wake-stator interaction tends to amplify the oscillations on the windward side of the airfoil and to momentarily extend their travelling distance. For configuration A, the amplitude of the oscillations is seen to increase and then decrease as the wake intersects and convects past the stator LE. The amplitude remains slightly higher than before wake approach, but decreases as the waves travel downstream. The distance travelled by the disturbances extends to about x/c = 0.15 (0.05c beyond the end of the patch) immediately after the wake intersects the stator LE, eventually shrinking back to half the patch length. A similar behavior is observed for the other configurations, although wave amplification seems to be proportional to the extension of the patch on the windward side. For configuration D, the oscillations are considerably amplified immediately after closest approach, momentarily travelling downstream over the entire

length of the patch. The amplitude diminishes somewhat with time, and the travelled distance is reduced to half the patch length (0.5 x/c).

Effect of Surface Porosity on Airfoil Unsteady Lift

The effect of wake passage on porous airfoil c_l is depicted in Figure 9. Note that, as for the solid case, the c_l is seen to decrease and then increase as the wake approaches and recedes from the stator, respectively. Several characteristics can be identified in the time histories, all direct consequences of the changes in effective geometry and increments in local flow unsteadiness brought about by porosity.

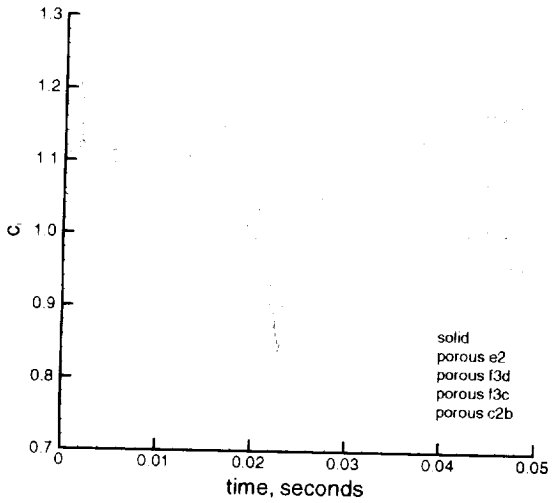

Figure 9.- Lift coefficient time histories for various porous airfoil configurations, medium grid level. $M_\infty = 0.166$, Re = 1.125×10^6, V = 78 c/s

Note from Figure 9 that the converged lift coefficient at the start of the traverse (t = 0.0 s) is different for all configurations. This is to be expected, since it is associated with different effective aerodynamic shapes. The average decrement in initial c_l ranges from approximately 4.5% to about 10% for configurations D and C, respectively. The average increment in airfoil drag coefficient at the start of the traverse (not shown) ranges from about 1% for configuration A to a drastic 50% for configuration D. The unsteadiness inherent in the flow as a result of porosity, which is represented by the amplitude of the small oscillations present in the time histories, appears to be proportional to the extent of the porous region. This trend, in conjunction with the alterations in effective geometry, is believed to be the cause of the changes in airfoil lift and drag previously noted.

It can also be observed from Figure 9 that, for the global period under consideration (~0.05 s), the lift coefficients associated with the porous configurations do not recover to the levels existing at the start of the wake traverse, unlike those for the solid airfoil. In general, this hysteresis effect seems to be proportional to the extent of porosity over the lower surface, and it may eventually disappear if longer periods are considered.

An attempt was made during the study to compare porosity effects on the basis of equal lift. To do so, the angle of attack of configuration A was increased until its c_l value at the start of the traverse matched the value corresponding to the solid airfoil. Since the increment in angle of attack was relatively large (approximately 2.5°), the resulting increment in drag was prohibitive, and the ability of porosity to reduce unsteady lift was diminished. It is apparent that, in order to compare on the basis of equal lift/drag, the shape of the airfoil would have to be redesigned/optimized including porosity. Such an undertaking is outside the scope of the present investigation.

Regardless of the changes in effective geometry and local flow, all the porous configurations being considered were able to reduce $(\Delta c_{l_w})_{max}$. This reduction, referenced to $(c_l)_0$, ranged from 16% to 26% for configurations B and D, respectively. Considering the changes in lift and drag coefficients at t = 0.0 s, $(\Delta c_l)_0$ and $(\Delta c_d)_0$, respectively, it appears that configuration A, with $(\Delta c_l)_0$ ~ -5% and $(\Delta c_d)_0$ ~ 1%, is the best performer with a reduction in unsteady lift of approximately 18% for the medium grid level results shown here. A fine grid solution, obtained for configuration A only, indicated that the reduction in unsteady lift could increase up to 21% with similar performance losses.

Concluding Remarks

The potential of passive porosity technology as a mechanism to reduce the unsteady lift on airfoils exposed to wake convection has been evaluated. To do so, a typical fan stator airfoil was immersed in a free field and subjected to the effects of a transversely moving wake. Solutions were obtained for a solid airfoil baseline, and for a series of porous configurations in order to identify those that would reduce unsteady lift without compromising airfoil performance. It was found that as long as the extension of the porous region on the leeward side did not exceed 10% of the chord, the flow over the entire airfoil surface remained attached. Despite a porosity-induced unsteady pattern of small inflow-outflow regions near the stator leading edge, it was determined that the use of porosity could reduce the magnitude of

the unsteady lift resulting from wake-stator interaction upwards of 18%, without incurring significant performance losses.

The work presented here constitutes the first stage of a study designed to assess the benefits of using passive porosity to reduce interaction noise in turbomachinery environments. The second stage of the study, which quantifies the reductions in unsteady lift in terms of changes in radiated rotor-stator interaction noise, will be presented in a future paper.

Acknowledgements

The authors wish to thank Dr. Christopher Rumsey, of the Computational Modeling and Simulation Branch at NASA LaRC, for his valuable advice and suggestions on the use of CFL3D.

References

1. Baines, W. D., and Peterson, E. G., "An Investigation of Flow Through Screens," Transactions of the ASME, July 1951.

2. Schubauer, G.B., Spangenberg, W. G., and Klebanoff, P.S., "Aerodynamic Characteristics of Damping Screens," NACA TN 2001, January 1950.

3. Dannenberg, R. E., Weiberg, J. A., and Gambucci, B. J., "The Resistance to Airflow of Porous Materials Suitable for Boundary Layer Control Applications using Area Suction," NACA TN 3094, December 1954.

4. Dannenberg, R. E., Gambucci, B. J. and Weiberg, J. A., "Perforated Sheets as a Porous Material for Distributed Suction and Injection," NACA TN 3669, April 1956.

5. Wood, R. M., Banks, D. W., and Bauer, S. X. S., "Assessment of Passive Porosity with Free and Fixed Separation on a Tangent Ogive Forebody," AIAA 92-4494, August 1992.

6. Chen, C., Chow, C., Van Dalsem, W. R., and Holst, T. L., "Computation of Viscous Transonic Flow over Porous Airfoils," J. of Aircraft, Vol. 26, No. 12, December 1989.

7. Gillian, M. A., "Computational Analysis of Drag Reduction and Buffet Alleviation on Viscous Transonic Flow over Porous Airfoils," AIAA 93-3419-CP, 1993.

8. Bauer, S. X. S., and Hemsch, M. J., "Alleviation of Side Force on Tangent-Ogive Forebodies Using Passive Porosity," AIAA 92-2711, June 1992.

9. Lee, S., "Effect of Leading Edge Porosity on Blade-Vortex Interaction Noise," AIAA 93-0601, January 1993.

10. Sugeng, F., and Fiedler, K., "An Experimental Investigation into Unsteady Blade Forces and Blade Losses in Axial Compressor Blade Cascade," Journal of Engineering for Gas Turbine and Power, Vol. 108, January 1986.

11. Lefcort, M. D., "An Investigation into Unsteady Blade Forces in Turbomachines," Transactions of the ASME, Journal of Engineering for Power, Vol. 87, October 1965.

12. Bush, R. H., "Engine Face and Screen Loss Models for CFD Applications," AIAA 97-2076, June 1997.

13. Cornell, W. G., "Losses in Flow Normal to Plane Screens," Transactions of the ASME, May 1958.

14. Frink., N. T., Bonhaus, D. L., Vatsa, V. N., Bauer, S. X. S., and Tinetti, A. F., "A Boundary Condition for Simulation of Flow over Porous Surfaces," AIAA 2001-2412, June 2001.

15. Krist, S. L., Biedron, R. T., and Rumsey, C. L., CFL3D User's Manual, Version 5.0, November 1996.

16. Roe, P. L., "Approximate Riemann Solvers, Parameter Vectors, and Difference Schemes," J. Comp. Phys., Vol. 43, No. 2, 1981, pp. 357-372.

17. Menter, F., "Zonal Two Equation k-ω Turbulence Models for Aerodynamic Flows," AIAA 93-2906, 1996.

18. Thomas, R. H., Gerhold, C. H., Farassat, F., Santa Maria, O. L., Nuckols, W. E., and DeVilbiss, D. W., "Far Field Noise of the 12 Inch Advanced Ducted Propeller Simulator," AIAA 95-0722, January 1995.

19. Mankbadi, R. R., "A Study of Unsteady Rotor-Stator Interactions", Transactions of the ASME, Journal of Turbomachinery, Vol. 111, October 1989.

20. Fujita, H., and Kovasnay, L. S., "Unsteady Lift and Radiated Sound from a Wake-cutting Airfoil," AIAA Journal, Vol. 12, No. 9, September 1974.

21. Bauer, S. X. S., private communication, May 2001.